Impairment of gamma-glutamyl transferase 1 activity in the metabolic pathogenesis of chromophobe renal cell carcinoma

Carmen Priolo[a,1], Damir Khabibullin[a], Ed Reznik[b,c], Harilaos Filippakis[a], Barbara Ogórek[a], Taylor R. Kavanagh[a], Julie Nijmeh[a], Zachary T. Herbert[d], John M. Asara[e], David J. Kwiatkowski[a], Chin-Lee Wu[f], and Elizabeth P. Henske[a]

[a]Pulmonary and Critical Care Medicine, Department of Medicine, Brigham and Women's Hospital and Harvard Medical School, Boston, MA 02115; [b]Department of Epidemiology and Biostatistics, Memorial Sloan–Kettering Cancer Center, New York, NY 10065; [c]Center for Molecular Oncology, Memorial Sloan–Kettering Cancer Center, New York, NY 10065; [d]Molecular Biology Core Facilities, Dana–Farber Cancer Institute, Boston, MA 02215; [e]Division of Signal Transduction, Department of Medicine, Beth Israel Deaconess Medical Center, Harvard Medical School, Boston, MA 02215; and [f]Department of Pathology, Massachusetts General Hospital, Harvard Medical School, Boston, MA 02114

Edited by Matthew G. Vander Heiden, Koch Institute at Massachusetts Institute of Technology, Cambridge, MA, and accepted by Editorial Board Member T. W. Mak February 15, 2018 (received for review June 15, 2017)

Chromophobe renal cell carcinoma (ChRCC) accounts for 5% of all sporadic renal cancers and can also occur in genetic syndromes including Birt–Hogg–Dube (BHD) and tuberous sclerosis complex (TSC). ChRCC has a distinct accumulation of abnormal mitochondria, accompanied by characteristic chromosomal imbalances and relatively few "driver" mutations. Metabolomic profiling of ChRCC and oncocytomas (benign renal tumors that share pathological features with ChRCC) revealed both similarities and differences between these tumor types, with principal component analysis (PCA) showing a distinct separation. ChRCC have a striking decrease in intermediates of the glutathione salvage pathway (also known as the gamma-glutamyl cycle) compared with adjacent normal kidney, as well as significant changes in glycolytic and pentose phosphate pathway intermediates. We also found that gamma glutamyl transferase 1 (GGT1), the key enzyme of the gamma-glutamyl cycle, is expressed at ∼100-fold lower levels in ChRCC compared with normal kidney, while no change in GGT1 expression was found in clear cell RCC (ccRCC). Significant differences in specific metabolite abundance were found in ChRCC vs. ccRCC, including the oxidative stress marker ophthalmate. Down-regulation of GGT1 enhanced the sensitivity to oxidative stress and treatment with buthionine sulfoximine (BSO), which was associated with changes in glutathione-pathway metabolites. These data indicate that impairment of the glutathione salvage pathway, associated with enhanced oxidative stress, may have key therapeutic implications for this rare tumor type for which there are currently no specific targeted therapies.

chromophobe RCC | oncocytoma | gamma-glutamyl cycle | glutathione | mitochondria

Renal cell carcinoma (RCC) is a morphologically and genetically heterogeneous malignancy (1, 2) arising from specialized cells in the nephron. The most common type is clear cell RCC (ccRCC), which represents 75–80% of RCC and derives its name from its clear cytoplasm on pathologic analysis. ccRCC is characterized by alterations at chromosome 3p, affecting the von Hippel–Lindau locus (3). The third most common renal cancer is the chromophobe RCC (ChRCC), representing about 5% of cases. ChRCC tend to have a more indolent clinical course compared with ccRCC, with the incidence of metastasis for ChRCC estimated at 6–7% (4). However, because there are currently no specific or proven therapies for metastatic ChRCC, the life expectancy for patients with metastatic ChRCC is estimated to be less favorable than for metastatic ccRCC (5).

ChRCC is pathologically distinctive because of striking accumulation of morphologically abnormal mitochondria (6, 7), which can result in a distinctive brownish color upon gross pathology and bright eosinophilic staining upon hematoxylin and eosin (H&E) staining. ChRCC can occur in two autosomal dominant genetic syndromes: Birt–Hogg–Dube (BHD) syndrome (8–10) and tuberous sclerosis complex (TSC) (11, 12). The pathogenic mechanisms underlying ChRCC are incompletely understood.

ChRCC often have multiple whole-chromosome losses, including chromosomes 1, 2, 6, 10, 13, 17, and 21 (13, 14). Interestingly, this pattern of genetic abnormality is not present in renal oncocytomas, benign renal tumors that share other pathological features with ChRCC, including the accumulation of mitochondria. ChRCC and oncocytomas cluster closely together upon analysis of gene expression profiles, consistent with their mitochondria-rich phenotype and their hypothesized origin from the distal nephron epithelium (15).

Two recent studies have reported comprehensive genomic and transcriptional analyses of ChRCC: The Cancer Genome Atlas (TCGA) (16), which analyzed 66 primary ChRCC tumors, and Durinck et al. (17), who analyzed 49 ChRCC. Both studies revealed a relatively quiet mutational landscape. While mutations in TP53 and genes in the PIK3CA pathway were detected in some tumors, the overall mutational burden was remarkably low, and nearly half of the tumors in both studies seem to lack an obvious "driver" mutation. These findings suggest that other pathogenetic mechanisms are involved. Interestingly, the TCGA

Significance

The mechanisms of chromophobe renal cell carcinoma (ChRCC) pathogenesis remain a key knowledge gap. Through metabolomics, this study uncovered a fundamental metabolic mechanism underlying the pathogenesis of ChRCC, with key therapeutic implications for this rare tumor type, for which there are currently no specific targeted therapies. Further understanding of the impact of glutathione salvage pathway on mitochondrial function, tumor progression, and targeted therapy can provide insight into other cancers characterized by aberrant glutathione salvage pathway.

Author contributions: C.P. and E.P.H. designed research; C.P., D.K., H.F., T.R.K., and J.M.A. performed research; B.O. and C.-L.W. contributed new reagents/analytic tools; C.P., D.K., E.R., Z.T.H., and D.J.K. analyzed data; and C.P., J.N., and E.P.H. wrote the paper.

Conflict of interest statement: M.G.V.H. and E.P.H. are both members of a clinical group at Dana–Farber Cancer Institute.

This article is a PNAS Direct Submission. M.G.V.H. is a guest editor invited by the Editorial Board.

[1]To whom correspondence should be addressed. Email: carmen_priolo@dfci.harvard.edu.

This article contains supporting information online at www.pnas.org/lookup/suppl/doi:10.1073/pnas.1710849115/-/DCSupplemental.

Published online June 11, 2018.

identified elevated expression of mitochondrial genes and mutations of mitochondrial DNA as characteristic features of ChRCC, with 18% of the tumors carrying heteroplasmic mutations in the mitochondrial genes ND1 or ND5, leading to the hypothesis that mitochondrial-driven metabolic mechanisms may be critical in the pathogenesis of ChRCC (18). However, the metabolic features of ChRCC are largely unknown, representing a key knowledge gap.

We have performed a metabolomic profiling of ChRCC. The most significantly altered metabolites identified between ChRCC and normal kidney are intermediates of glucose metabolism (including glucose-6-phosphate, lactate, and 6-phosphogluconate) and gamma-glutamyl amino acids (including gamma-glutamyl alanine, gamma-glutamyl leucine, and gamma-glutamyl methionine). Gamma-glutamyl amino acids are key intermediates of the gamma-glutamyl cycle, which is critical to the response to oxidative stress. This defect in glutathione salvage is linked to strikingly lower levels of the gamma-glutamyl transferase 1 (GGT1) in ChRCC, relative to normal kidney and to ccRCC. GGT1 is a membrane transpeptidase that removes the gamma-glutamyl moiety from extracellular glutathione (GSH), GSSG, or GSH conjugates and transfers it to an amino acid acceptor, thereby creating a gamma-glutamyl amino acid. These gamma-glutamyl amino acids are transported into the cytoplasm together with cysteine and glycine, the other components of the tripeptide glutathione. The gamma-glutamyl cycle helps to maintain intracellular GSH levels, leading this to be referred to as the "glutathione salvage" pathway. This highly specific defect in GGT1 suggests that impairment of the glutathione salvage pathway may act as an "Achilles' heel" of ChRCC, leading to increased sensitivity to oxidative stress, mitochondrial damage, and reprogramming of glutamine and glucose metabolism. Consistent with this hypothesis, down-regulation of GGT1 sensitizes cells to oxidative stress. This vulnerability may represent an opportunity for the development of specific therapies for metastatic and recurrent ChRCC.

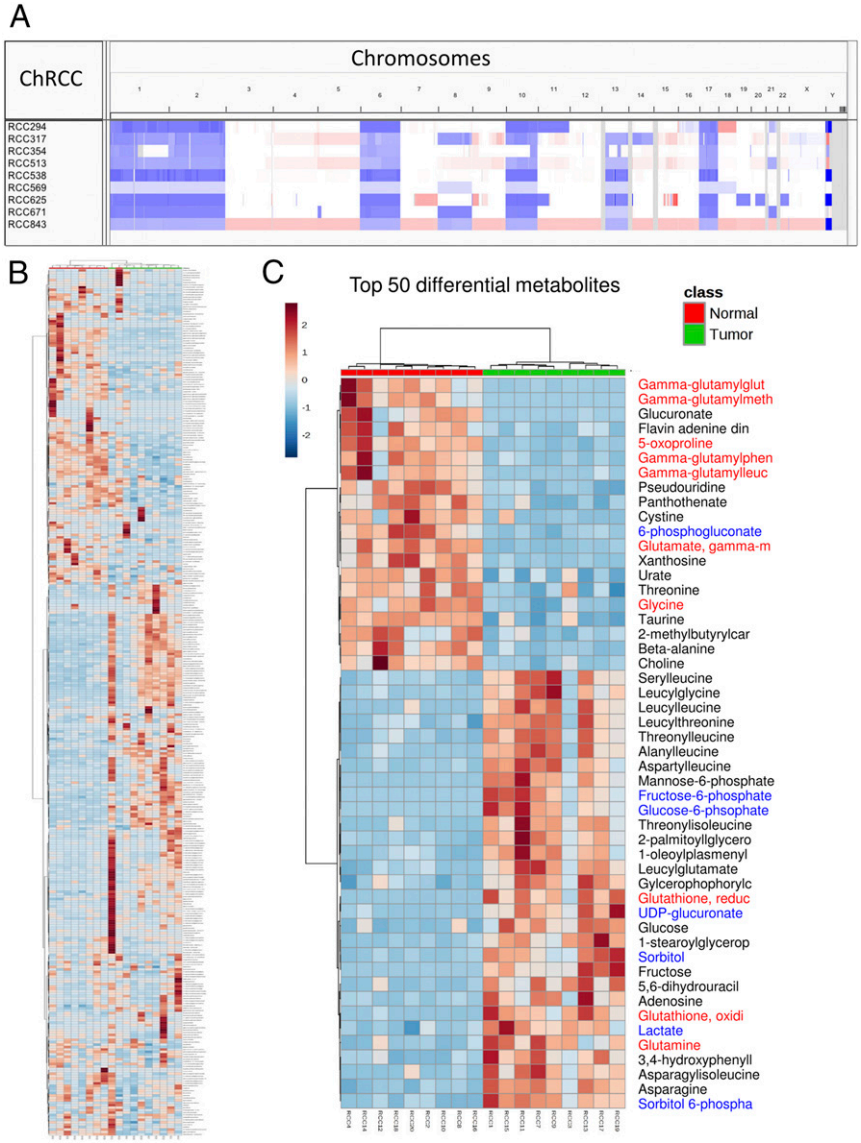

Fig. 1. Chromosome copy number and metabolite profiles of ChRCC specimens. (*A*) Tumors show multiple chromosomal losses (blue regions: 1, 2, 6, 8, 10, 13, 17), consistent with previous studies. (*B*) Unsupervised clustering of ChRCC and adjacent normal kidney metabolite profiles. All of the measured metabolites (n = 367) are depicted. (*C*) The top 50 differential metabolites (by P value) between ChRCC and normal kidney included intermediates of glucose (blue highlighted) and glutathione (red highlighted) metabolic pathways. Heatmaps were generated using MetaboAnalyst.

Results

Whole-Exome Sequencing Reveals Distinctive Chromosomal Losses and a Low Somatic Mutation Rate. Nine fresh frozen ChRCC tissue samples and adjacent normal kidney were studied. H&E staining of frozen sections was used to confirm the diagnosis and exclude necrotic areas. Whole-exome sequencing revealed a low somatic mutation rate (15–40 somatic mutations per tumor), including p53 mutations in three cases (c.524G > A; c.469G > T; c.672_splice) and mutations in components of the PI3-kinase pathway in two cases (PTEN, c.546_549delAAAG; c.591_593delGAT; and PIK3CA, c.3130A > T). Copy number inferred from whole-exome data revealed whole chromosome loss in most tumors (Fig. 1*A*), including losses of chromosomes 1, 2, 6, 8, 10, 13, and 17 in the majority of tumors, similar to the TCGA dataset (18).

Hierarchical Clustering Analysis of Metabolomic Data Segregates ChRCC and Their Normal Counterparts. Mass spectrometry-based metabolomics was conducted on the ChRCC and normal kidney. An average of 367 known metabolites were detected and measured using a liquid chromatography/gas chromatography platform (Metabolon Inc.). Tumors and normal samples were ordered by unsupervised clustering. The tumors were clustered together and separated from the normal kidney samples (Fig. 1*B*). Raw and mass-normalized values, fold changes (tumor to normal), and *q* values for all metabolites are included in Dataset S1.

Aberrant Glucose and Glutathione Metabolism in ChRCC. Analysis of the top 50 differential metabolites between ChRCC and normal kidney revealed striking changes in intermediates of glucose and glutathione metabolism (Fig. 1*C*), which included the following: (*i*) intermediates of glycolysis (glucose-6-phosphate, fructose-6-phosphate, and lactate) and the pentose phosphate pathway (sedoheptulo-7-phosphate, 6-phosphogluconate); (*ii*) UDP-glucuronate, a glucose derivative and precursor of vitamin C; and (*iii*) intermediates of glutathione biosynthesis (glutathione, glutamine, glutamate, glycine) and glutathione salvage (gamma-glutamyl amino acids, 5-oxoproline). Vitamin C and glutathione represent major determinants of the cell redox state. Interestingly, ophthalmate, a biomarker of oxidative stress (19, 20), was increased by ∼eightfold in ChRCC vs. normal kidney. Ophthalmate is an analog of glutathione that is synthesized by glutathione biosynthetic enzymes using 2-amino butyric acid as a precursor.

A volcano plot was generated to identify the most significant metabolites by both fold change (±2; *x* axis) and *P* value ($P < 0.01$; *y* axis; Fig. 2*A*). Of 36 metabolites decreased in ChRCC vs. normal kidney (Dataset S2), 9 belonged to glutathione metabolism, primarily the gamma-glutamyl cycle (glutathione salvage pathway) (Fig. 2*B*). The components of glutathione metabolism that were decreased in ChRCC included seven gamma-glutamyl amino acids (gamma-glutamylphenylalanine, gamma-glutamylglutamate, gamma-glutamylalanine, gamma-glutamylleucine, gamma-glutamylisoleucine, gamma-glutamylmethionine, and gamma-glutamylvaline) and the cyclic glutamate derivative 5-oxoproline

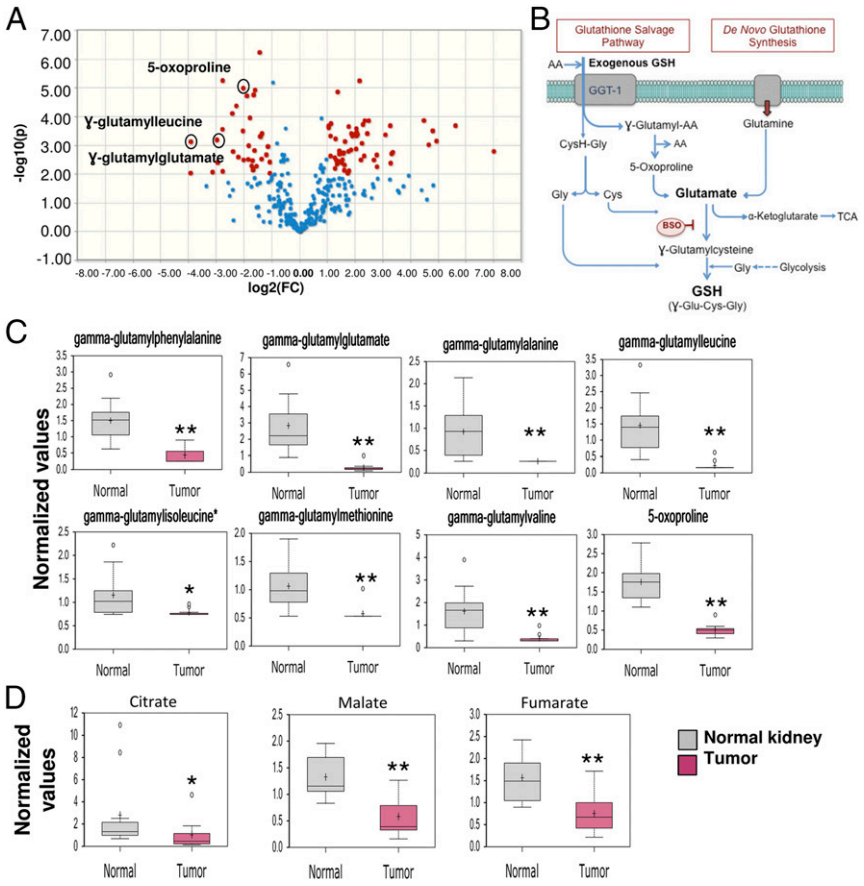

Fig. 2. Gamma-glutamyl cycle intermediates are among the top differential metabolites in ChRCC versus normal kidney. (*A*) Both fold changes (FC, *x* axis; threshold 2) and *P* values (*y* axis; threshold 0.01) are log-transformed. Red circles represent significant metabolites. The further the red circle is away from the (0,0), the more significant the feature is. (*B*) Graphical representation of the glutathione synthetic pathways. BSO, buthionine sulfoximine. (*C*) Boxplots showing normalized values of glutathione salvage pathway intermediates significantly down-regulated in ChRCC vs. normal kidney. (*D*) Boxplots showing significantly lower TCA cycle intermediates in ChRCC vs. normal kidney. Median scaling was applied. $*P < 0.05$; $**P < 0.01$.

(Fig. 2*C*). Gamma-glutamyl amino acids are direct products of GGT1, the key enzyme of the gamma-glutamyl cycle. The glutathione salvage pathway is critical for intracellular incorporation of amino acids, mainly glutamyl and cysteine moieties, for glutathione regeneration.

One of the main pathologic hallmarks of ChRCC is increased mitochondrial mass and aberrant mitochondrial morphology. Interestingly, our metabolomics dataset showed a significant decrease in TCA cycle intermediates in ChRCC relative to normal kidney, including citrate ($P < 0.05$), malate, and fumarate ($P < 0.01$) (Fig. 2*D*), suggesting mitochondrial dysfunction, which may also contribute to enhanced oxidative stress.

Consistent with both metabolite analyses, a pathway enrichment analysis identified gamma-glutamyl amino acid and the pentose phosphate pathways among the seven metabolite sets with top enrichment scores (Dataset S3).

As noted earlier, oncocytomas are benign renal tumors that share certain pathologic features with ChRCC, including the accumulation of aberrant mitochondria and presumed origin in the distal nephron. Interestingly, metabolomic profiling of oncocytomas ($n = 10$, with adjacent normal kidney; Dataset S4) revealed both similarities and striking differences from the ChRCC. First, a principal component analysis (PCA) revealed a distinct separation between oncocytomas and ChRCC samples (Fig. S1*A*). Second, in contrast to ChRCC, glycolysis and the pentose phosphate pathway were not significantly changed in oncocytomas compared with matched normal kidney, as shown by pathway enrichment analysis and relative abundance (Fig. S1*B* and Datasets S3 and S5). Similarly to ChRCC, oncocytomas showed markedly elevated levels of GSH and GSSG (Fig. 3*B* and Table 1), and decreased levels of TCA metabolites (Dataset S4), consistent with mitochondrial impairment. Oncocytomas have been shown to harbor mitochondrial mutations (21, 22). In addition, 12 of 17 measured gamma-glutamyl amino acids were decreased in oncocytomas, but 3 were significantly increased, suggesting a partially functional glutathione salvage pathway (Fig. 3*C*, Table 1, and Dataset S4).

Next, we compared the ChRCC and oncocytoma metabolomics datasets with published ccRCC metabolomics data (23) generated using the same platform. PCA showed clear separation of ccRCC from ChRCC and oncocytoma (Fig. 3*A*), and relative abundance analysis revealed specific differences in gamma-glutamyl amino acids and acylcarnitines. The pattern of changes in gamma-glutamyl amino acids was similar between ccRCC and oncocytomas, with some gamma-glutamyl amino acids significantly elevated in ccRCC compared with normal

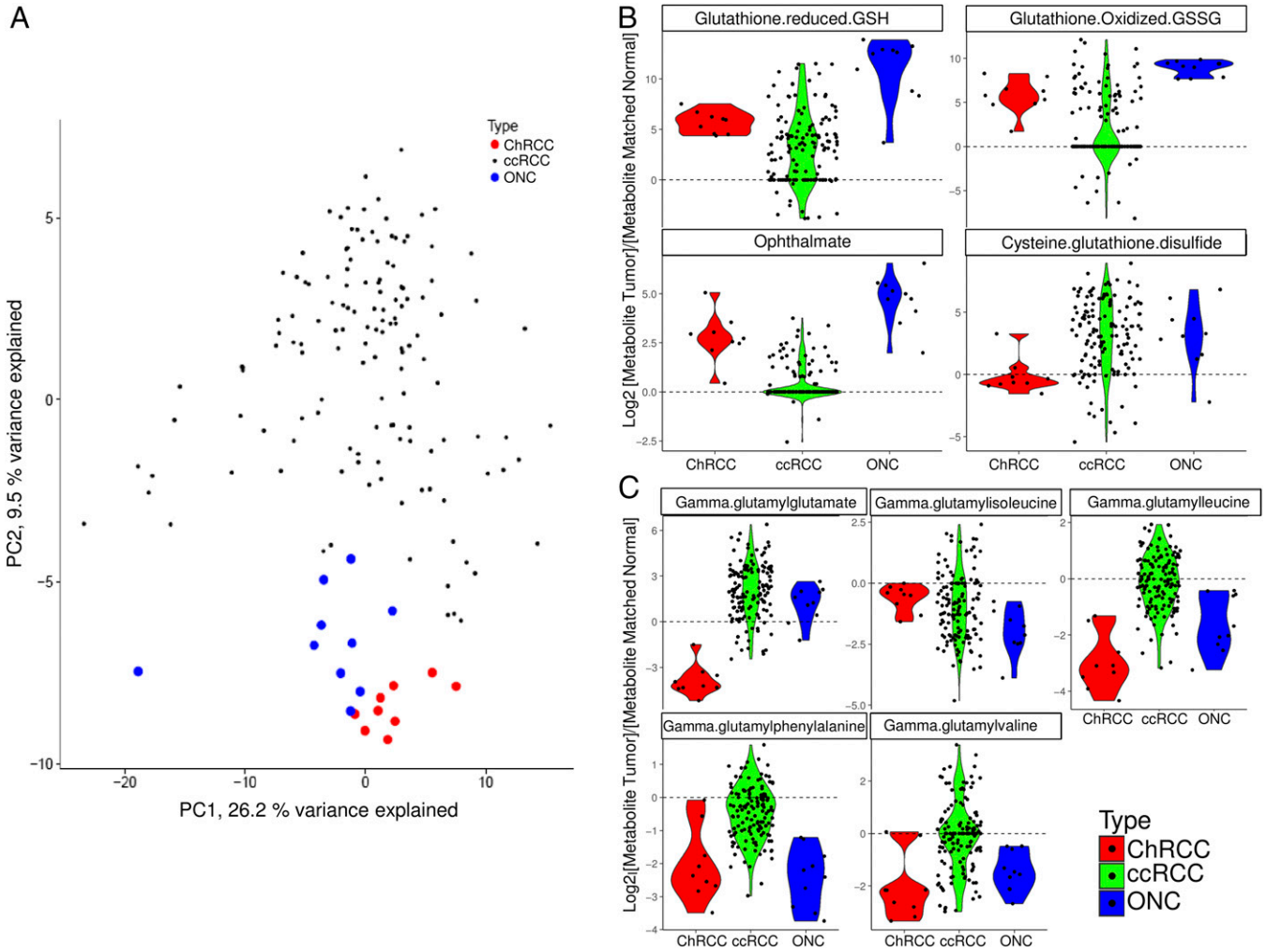

Fig. 3. PCA reveals separation of ChRCC, oncocytomas, and ccRCC. (*A*) PCA of merged metabolomics data from a published ccRCC dataset (23) (black dots) and chromophobe (red dots) and oncocytoma (blue dots) datasets in this study. Data were merged by calculating the $\log_2$ ratio of metabolite levels in tumors to matched normal samples for all datasets. Boxplots of $\log_2$ tumor/normal ratios of glutathione-related metabolites, oxidative stress markers (*B*), and gamma-glutamyl amino acid species (*C*) across ChRCC, ccRCC, and oncocytoma samples are shown.

Table 1. Glutathione-related metabolites analyzed in oncocytomas compared with matched normal kidney

Metabolites	Tumor/normal	*q* value
Glutathione, reduced (GSH)	192.83*	0.0000005
Glutathione, oxidized (GSSG)	566.29*	0
Cysteine-glutathione disulfide	3.32*	0.013
S-methylglutathione	5.83*	0.0009
Cysteinylglycine	12.85*	0.0000045
5-oxoproline	0.61†	0.0003
Ophthalmate	33.73*	0.0000054
Gamma-glutamylalanine	0.43†	0.0032
Gamma-glutamylcysteine	14.14*	0.0007
Gamma-glutamylglutamate	2.11*	0.012
Gamma-glutamylglutamine	3.27*	0.0296
Gamma-glutamylglycine	0.23†	0.0003
Gamma-glutamylhistidine	0.34†	0.0000017
Gamma-glutamylisoleucine	0.27†	0.0000215
Gamma-glutamylleucine	0.37†	0.0002
Gamma-glutamyl-alpha-lysine	0.32†	0.000047
Gamma-glutamyl-epsilon-lysine	1.03	0.3252
Gamma-glutamylmethionine	0.48†	0.007
Gamma-glutamylphenylalanine	0.19†	0.0000052
Gamma-glutamylthreonine	0.38†	0.0000052
Gamma-glutamyltryptophan	0.9	0.1961
Gamma-glutamyltyrosine	0.23†	0.0000005
Gamma-glutamylvaline	0.38†	0.0000307
Gamma-glutamylserine	0.4†	0.0006

*Metabolites that were significantly increased.
†Metabolites that were significantly decreased (n = 10).

kidney. Several acylcarnitines, which are involved in fatty acid transfer into the mitochondria for fatty acid oxidation, were significantly elevated in ccRCC (Fig. 3*C*, Fig. S1*C*, and Dataset S5). Finally, markers of oxidative stress, such as ophthalmate and cysteine glutathione disulfide, were differentially elevated in the three tumor types, with ophthalmate significantly elevated in ChRCC and oncocytoma, and cysteine glutathione disulfide significantly elevated in ccRCC and oncocytoma (Fig. 3*B* and Dataset S5).

Low Expression of GGT1 in ChRCC. Given the significant change in gamma-glutamyl amino acids and other metabolites of the glutathione salvage pathway in ChRCC, we examined the expression of GGT1 (the key enzyme in this pathway; Fig. 2*B*) in ChRCC using RNA-seq data from the TCGA (66 ChRCC and 25 normal kidney samples) (18). GGT1 mRNA was >100-fold lower in chromophobe RCC compared with normal kidney. In contrast, in the ccRCC TCGA dataset (82 ccRCC and 18 normal kidney samples) (24), no difference in GGT1 was observed between ccRCC and normal kidney (Fig. 4*A*). These data suggest that low GGT1 expression may be the mechanism underlying the metabolic changes in the gamma-glutamyl cycle in ChRCC and further distinguish ChRCC from ccRCC.

To further confirm this, we measured GGT1 expression in spontaneously immortalized cells (ChromoA) derived from a sporadic ChRCC (25), compared with human epithelial kidney HK2 cells and human embryonic kidney HEK293 cells. GGT1 levels in the ChromoA cells were very low (Fig. 4*B*). A second primary cell line (Chromo 1039) we derived from a ChRCC also had almost undetectable expression of GGT1 mRNA compared with primary culture of normal kidney from the same patient (Fig. 4*C*). Both ChromoA and Chromo1039 cells exhibited the typical chromosomal changes of ChRCC as seen via single-nucleotide polymorphism (SNP) array analysis of genomic DNA, with loss of chromosomes 1, 2, 6, 10, and 13 in both tumors, and the Chromo1039 maintained genomic features of the parental tumor sample from which it was derived (Fig. 4 *D*–*F*).

To validate the differential role of GGT1 in ChRCC versus ccRCC, we queried the cancer cell line encyclopedia (CCLE) (26) using the Oncomine database (27) and found that ccRCC cell lines (n = 21) have the highest GGT1 expression levels across 18 different cancer cell types ($P < 0.001$, fold change = 6.8; Fig. S2*A*). Interestingly, down-regulation of GGT1 led to decreased viability in the ccRCC-derived 786-O cell line, suggesting a prosurvival role of GGT1 in ccRCC (Fig. S2 *B* and *C*).

GGT1 Down-Regulation Sensitizes Normal Kidney Cells to Inhibition of Glutathione Synthesis. Next, we analyzed gene expression levels of other genes of the glutathione pathway in the ChRCC and ccRCC TCGA. Expression of glutamate-cysteine ligase catalytic subunit (GCLC), glutathione synthetase, and SLC7A11, which encodes xCT (a component of an amino acid transport system highly specific for cysteine and glutamate where the anionic form of cysteine is transported in exchange for glutamate), was significantly higher in ChRCC compared with normal kidney but not in ccRCC compared with normal kidney (Fig. 5*A* and Fig. S2*F*).

Based on these findings, we hypothesized that low GGT1 activity in ChRCC leads to dependency on de novo glutathione synthesis and increased susceptibility to oxidative stress. Importantly, GCLC can be specifically targeted with an irreversible inhibitor, buthionine sulfoximine (BSO). To test our hypothesis, GGT1 was down-regulated using smart pool siRNA or three individual siRNA in HEK293T cells (Fig. 5*B* and Fig. S3 *A*–*C*). The cells were treated with H_2O_2 (100 μM) and/or BSO (50–400 μM). Treatment with the combination of H_2O_2 and BSO for 48 h significantly suppressed ATP production in siGGT1 as measured by CellTiter-GLo luminescence (Fig. 5*C* and Fig. S3 *A*–*C*), confirming that loss of GGT1 enhances susceptibility to oxidative stress. This effect appears specific to oxidative stress since differential sensitivity was not observed in response to ER stress (induced by treatment with tunicamycin) or osmotic stress (induced by sorbitol) between siGGT1 and siControl (Fig. S3*D*). Furthermore, ChRCC-derived ChromoA cells showed increased sensitivity to BSO upon hydrogen peroxide challenge ($P < 0.001$), whereas no synergistic effect of the combination was found in ccRCC-derived 786-O cell line (Fig. S2 *D* and *E*).

GGT1 Down-Regulation Induces Metabolic Rewiring Involving Glucose and Glutamine Pathways. To more specifically elucidate the impact of oxidative stress and BSO treatment on cells with low GGT1, we analyzed the metabolome of HEK293T cells with siGGT1 or siControl, with or without a 24-h H_2O_2 (100 μM) challenge. Unsupervised clustering revealed distinct changes upon GGT1 down-regulation (Fig. 6*A*). The top 50 metabolites significant by ANOVA included glutamine, glutamate, GSSG, and arginine (Fig. 6*B* and Dataset S6). Glutamine, glutamate, and GSSG were significantly increased in siGGT1 cells versus siControl (Fig. 6*B*). Both glutamine and glutamate decreased significantly in siGGT1 cells after challenge with H_2O_2, consistent with higher consumption in response to oxidative stress (Fig. 6*B*). Interestingly, glutamine, glutamate, and arginine were also among the top five most significantly up-regulated metabolites in siGGT1 vs. siControl cells (comparison of two groups by FDR). Arginine is an amino acid known to be involved in the response to oxidative stress. A separate analysis of the impact of H_2O_2 revealed that intermediates of glycolysis and the pentose phosphate pathway (PPP) were among the top elevated metabolites in siGGT1 + H_2O_2 vs. siGGT1 cells (Fig. 6*C*). Finally, we overexpressed GGT1 in HEK293T cells (Fig. 6*E*) and performed metabolite analysis on these cells (Dataset S7). Significance analysis of microarray (SAM) revealed association of GGT1 overexpression with an increase in 5-oxoproline, consistent with enhanced gamma-glutamyl transferase activity, and a decrease in

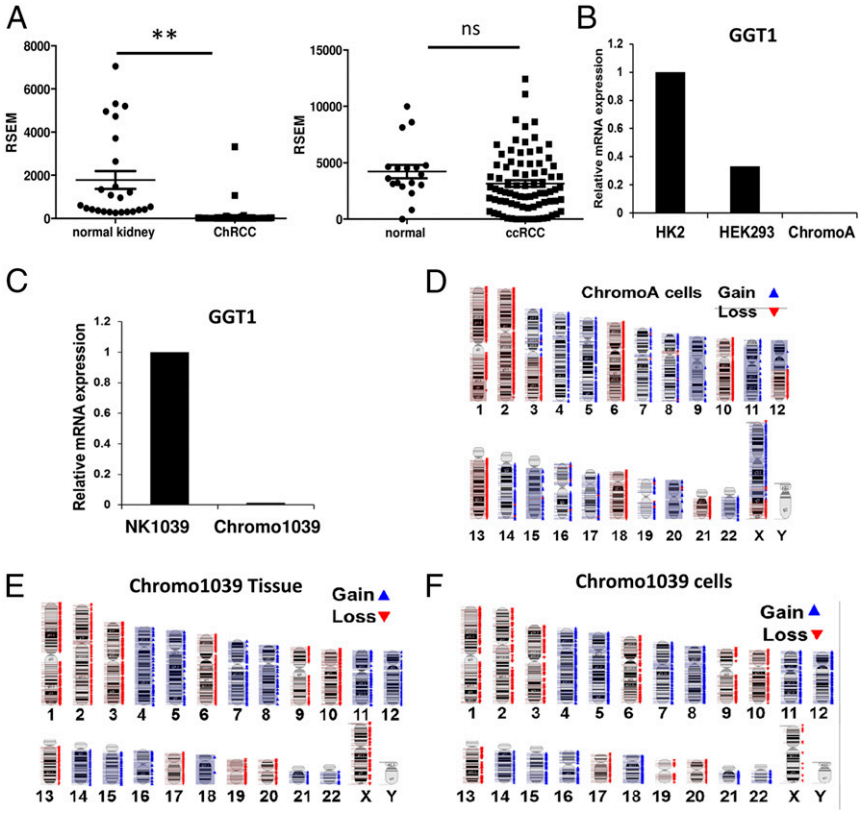

Fig. 4. Low GGT1 expression in ChRCC tumors and tumor-derived cells. (*A*) GGT1 expression is low in ChRCC compared with normal kidney but not in ccRCC. Transcript quantification is expressed as RSEM and was obtained through analysis of the TCGA datasets. Mann–Whitney test was applied, $^{**}P < 0.01$; ns, not significant. (*B*) GGT1 mRNA is low in ChRCC-derived ChromoA cells compared with HK2 and HEK293T cells. (*C*) GGT1 mRNA is lower in primary Chromo1039 cells compared with primary normal kidney cultures from the same patient (NK1039). (*D–F*) SNP arrays show typical aneuploidy in ChromoA cells (*D*), Chromo1039 tumor tissue (*E*), and primary cultured cells from the Chromo1039 tumor (*F*).

both GSH and GSSG (Fig. 6*D* and Dataset S7), suggesting that GGT1 may accelerate glutathione turnover.

Discussion

Chromophobe RCC are very unusual tumors, with abundant abnormal mitochondria and a low rate of driver mutations in their genomic DNA, leading to the hypothesis that the fundamental driver of ChRCC pathogenesis involves metabolic dysregulation. However, the factors that initiate this hypothesized metabolic dysregulation are largely unknown. We have performed a metabolomic profiling of ChRCC, revealing an unexpected defect in the gamma-glutamyl cycle. Intermediates of the gamma-glutamyl cycle, including gamma-glutamyl alanine, gamma-glutamyl leucine, and gamma-glutamyl methionine, were strikingly decreased in ChRCC compared with normal kidney, in addition to the cyclic glutamate derivative 5-oxoproline. Gamma-glutamyl amino acids are key intermediates in the gamma-glutamyl cycle, which is also called the glutathione salvage pathway. In ChRCC, this defect in gamma-glutamyl amino acids appears to be mediated by GGT1, the key enzyme of this pathway. GGT1 is expressed at ∼100-fold lower levels in ChRCC vs. normal kidney in TCGA dataset. In contrast, no difference in GGT1 is seen in ccRCC compared with normal kidney. We also found very low levels of GGT1 in two primary cultures of ChRCC compared with normal kidney. The mechanisms of GGT1 down-regulation in ChRCC will require further investigation. There is no evidence of loss of the GGT1 gene locus, which is on chromosome 22q21, in ChRCC.

GGT1 is a membrane transpeptidase expressed primarily on the apical surface of cells of the kidney and liver, allowing for intracellular incorporation of amino acids, including glutamyl and cysteine moieties for glutathione regeneration. In the setting of oxidative stress, we hypothesize that GGT1-deficient cells would reprogram their metabolism to enhance endogenous GSH synthesis through activation of other pathways to compensate for their inability to "recycle" extracellular GSH, including directing glutamine and glutamate toward GSH synthesis instead of the TCA anaplerotic reaction (α-ketoglutarate), and enhancing the PPP. This is consistent with our metabolomics data, which revealed not only defects in the glutathione salvage pathway, but also low levels of TCA cycle intermediates and changes in glucose-related metabolites, including several PPP intermediates.

GGT1 deficiency in the liver has been reported to induce swollen mitochondria (28), and increased mitochondrial mass and dysmorphic (and often swollen) mitochondria are pathologic hallmarks of ChRCC. We hypothesize, therefore, that the enhanced oxidative stress in ChRCC is linked to the accumulation of these dysfunctional mitochondria, leading to a vicious cycle of oxidative stress, leading to dysfunctional mitochondria, leading to further oxidative stress. A key question is whether these abnormal mitochondria in ChRCC are functional. The ChRCC TCGA found mutations in ETC complex 1 genes in 18% of cases, with *MT-ND5* (essential for complex 1 activity) being the most frequently altered gene (18), but whether these mutations are a cause or an effect of the mitochondrial dysfunction is unclear. We found lower levels of mitochondrial metabolites of the TCA cycle, including citrate, malate, and fumarate, in ChRCC compared with normal kidney. This finding suggests that the mitochondria are dysfunctional. Whether the accumulation of mitochondrial DNA mutations in a subset of ChRCC is a potential consequence of GGT1 deficiency is unknown.

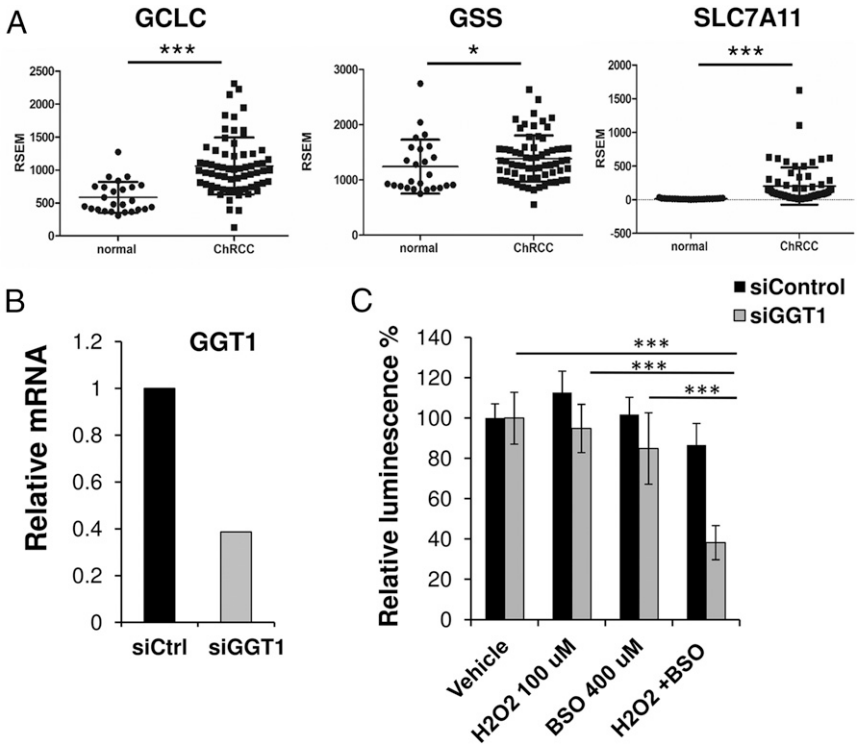

Fig. 5. GGT1 down-regulation sensitizes kidney cells to treatment with H_2O_2 and BSO. (*A*) Low expression of GCLC, glutathione synthetase (GSS), and SLC7A11, which encodes xCT, in ChRCC vs. normal kidney (TCGA RNA seq datasets). Mann–Whitney test was applied. (*B*) Lower GGT1 expression in HEK293T cells following 72-h transfection with GGT1 smart pool siRNA (gray bars) compared with control siRNA (black bars). (*C*) CellTiter-Glo luminescence was measured in HEK293 cells after 48-h treatment with H_2O_2 and/or BSO. Data shown is representative of three experiments. Two-way ANOVA test followed by Bonferroni correction was applied. $*P < 0.05$; $***P < 0.001$.

Interestingly, the metabolite profile of oncocytomas, which are known to harbor mitochondrial DNA mutations impairing mitochondrial respiration (21, 22), revealed similar changes in TCA cycle intermediates, supporting our hypothesis that mitochondria are dysfunctional in ChRCC. The reasons that dysfunctional mitochondria accumulate to such high levels in ChRCC are not known but may be linked to prior findings in oncocytomas by Eileen White and coworkers (29). Oncocytomas are benign tumors that appear to be closely related to ChRCC: They are also thought to arise from the distal nephron and they accumulate abundant aberrant mitochondria. It is intriguing that a prior study found that ChRCC ($n = 9$) and oncocytomas ($n = 11$) have low GGT1 expression by immunohistochemistry relative to ccRCC ($n = 31$) (30). In oncocytoma, defective mitophagy leads to the accumulation of abnormal mitochondria, but in the setting of wild-type *p53*, tumorigenesis is suppressed, resulting in a benign phenotype. Subsequent mutations in *p53* are hypothesized to restore growth capacity and enable progression from oncocytoma toward chromophobe RCC (29); in this model, oncocytomas represent a precursor lesion for ChRCC. However, despite their pathologic similarities, our data point toward clear differences in the metabolome of ChRCC versus oncocytomas, with oncocytomas showing no changes in glycolysis and PPP intermediates and higher levels of certain gamma-glutamyl amino acids.

Currently, nearly all patients with metastatic or unresectable ChRCC will die of their disease. Therapies proven to have efficacy in ccRCC are often utilized in the treatment of ChRCC, despite the fact that ChRCC are genetically, transcriptionally, and, as we have now shown, metabolically distinct from ccRCC. The insights from this study may lead to specific targeted therapies for ChRCC, taking advantage of their fundamental vulnerability to oxidative stress. Understanding the impact of the glutathione salvage pathway on mitochondrial function and cellular redox status may also elucidate the metabolic pathogenesis of other human malignancies.

Materials and Methods

Tumor Samples. RCC specimens and adjacent normal kidney were obtained from the Massachusetts General Hospital, with approval of the Partners Institutional Review Board. Samples were flash-frozen within 30 min of surgical dissection.

Whole-Exome Sequencing and Copy Number Analysis. Exome sequencing was performed by the Broad Institute Genomics Platform and analyzed using a standard analytic pipeline deployed in the Firehose environment. Exome capture targeted 33 Mb in 193,094 exons in 18,863 genes. Briefly, reads were aligned using bwa, followed by indel realignment and quality score recalibration using the Genome Analysis Toolkit (31). Somatic mutations were identified from tumor-normal pairs using MuTect (32) and Indelocator [www.broadinstitute.org/cancer/cga/indelocator]. Copy number profiles were derived from fractional coverage values of each exon compared with a panel of normals using Cap-Seg (https://github.com/aaronmck/CapSeg) and Allelic-CapSeg in the Clonal Evolution Exome Suite in the Firehose environment.

Analysis of TCGA RNA-Seq Data. RNA-seq data were obtained from The Broad Institute Firehose pipeline (gdac.broadinstitute.org). RNA-seq samples were aligned using the UNC RNA-seq V2 pipeline, and RSEM values for each gene were generated using TCGA standard protocols (16). For ChRCC, 66 tumors and 25 matched normal tissue samples were used (18). For ccRCC, 82 tumors and 18 normal tissue samples were used (24).

SNP Arrays. Two hundred fifty nanograms of DNA extracted from ChRCC and matched normal kidney primary cells and parental tumor and normal tissue samples were labeled and hybridized to the Affymetrix 250K Nsp array to obtain signal intensities and genotype calls (Microarray core facility, Dana–Farber Cancer Institute). The array image was acquired using Affymetrix GeneChip Command Console Software. Copy number values for individual SNPs were

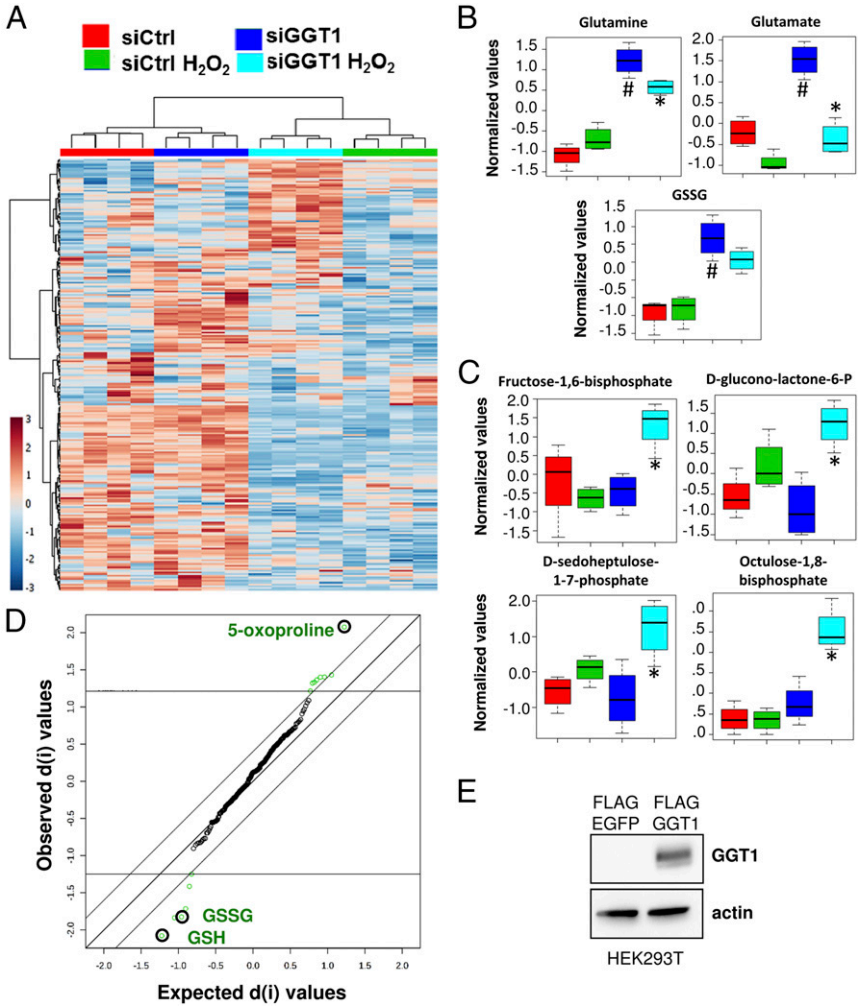

Fig. 6. Metabolic changes induced by GGT1 down-regulation or overexpression. (*A*) Heatmap depicting unsupervised clustering of HEK293T cells transfected with siCtrl or siGGT1 ± H_2O_2 (four samples per group; 281 metabolites) was generated with MetaboAnalyst. (*B* and *C*) Box plots of normalized values show increased levels of glutamine and glutamate induced by inhibition of GGT1 (blue) compared with control siRNA (red) (*B*) and enhanced glycolytic and PPP intermediates upon 24-h treatment of the GGT1-depleted cells with H_2O_2 (turquoise) vs. H_2O_2 treatment of the control siRNA (green) (*C*). ANOVA followed by Tukey's post hoc test was applied. *$P < 0.05$ vs. siGGT1; #$P < 0.05$ vs. control (siCtrl). SAM shows significant metabolites ($n = 14$) for delta 0.4 (FDR = 0.079, false positive 1.77) (*D*) in HEK293T cells overexpressing GGT1 (FLAG-GGT1) vs. control (FLAG-EGFP) (*E*).

extracted and converted from CEL files into signal intensities using Affymetrix Genotyping Console 4.2.026 using the BRLMM algorithm. Copy number and loss of heterozygosity (LOH) analysis was conducted using Affymetrix Copy Number Analysis Tool (CNAT). Genomic smoothing analysis was performed by using the smoothing window of 0.1 Mb, and inferred copy number states were derived from a Hidden Markov Model-based algorithm implemented in CNAT. ChromoA cells were compared with 49 normal samples from the Mapping 500K HapMap Genotype Data Set with 24 females and 25 males. Parental tumor and primary Chromo 1039 cells were paired to determine copy number variance.

Metabolite Profiling. Extraction and profiling of metabolites from ChRCC, oncocytomas, and matched normal kidney tissue samples was conducted at Metabolon Inc. as previously described (23, 33). Following peak identification and QC processing, metabolite values were normalized by tissue weight for each sample and median scaling of each metabolite across all samples and imputation of each metabolite by the minimum observed value of that compound were performed (33).

Pathway enrichment analysis was conducted using MetaboLync (Metabolon Inc). Metabolite sets including <2 measured metabolites were excluded.

To compare metabolite data from the ChRCC, oncocytoma, and ccRCC (23) datasets, we first calculated the $\log_2$ ratio of abundance in tumor to abundance in matched normal tissue sample for each metabolite in each patient across all datasets. This transformation enabled us to merge the metabolomics data for ChRCC, oncocytoma, and ccRCC tumors into one merged dataset. This dataset was then used for PCA.

Differential abundance of a metabolite was estimated as the average $\log_2$-fold change across all relevant samples. A Wilcoxon signed rank test was used to determine statistical significance. *P* values were adjusted using the Benjamini–Hochberg method, with a threshold of $q < 0.1$ for statistical significance. Metabolite profiling of HEK293T cells with and without GGT1 downregulation or overexpression was performed using an LC-MS platform (34). Raw data were normalized to total proteins and scaling (values where meancentered and divided by the SD of each metabolite) was applied. Heat map generation, ANOVA, and SAM statistical analyses were conducted using MetaboAnalyst (www.metaboanalyst.ca/) (34, 35).

Cell Lines, siRNA, and Drug Treatment. HK2, HEK293T, 786-O, and ChromoA (25) cells were grown in DMEM with 10% FBS. Chromo1039 primary cells were derived from a histologically confirmed ChRCC and compared at passage 2 to normal primary cells cultured from the same kidney. To establish the primary culture, tissues were minced into small pieces. Fractional digestions were performed using collagenase type I solution (1 mg/mL; Sigma). The normal kidney cells were then plated in Keratinocyte SFM medium (Gibco 10724-011) and the RCC cells (Chromo 1039) in DMEM/F12 (Gibco 1132-033). The RCC cells were subsequently cultured in a 1:1 mix of Keratinocyte media with DMEM supplemented with 10% FBS. For the siRNA experiments, HEK293T or 786-O cells were transfected for 72 h with GGT1 smart pool siRNA, individual siRNAs

comprising the pool [all purchased from GE Dharmacon; target sequences: J-005884-18 (GCUCGAAGAUUGGGAGGGA), J-005884-19 (UACAACAGCACCACACGAA), J-005884-20 (ACGAGACGCUGGCCAUCGA), J-005884-21 (CUGUCUUGUGUGAGGUGUU)], or other individual siRNAs (Silencer Select siRNA s5724, Ambion; target sequences: s5724 (UGGUUGUCAGGUUCCUUGG). Cells were grown on 96-well white opaque plates (Corning, catalog no. 353296). CellTiter-Glo luminescence was measured after 48 h of treatment with H_2O_2 and/or BSO (Sigma B2515, freshly dissolved before each experiment) to induce oxidative stress, tunicamycin to induce ER stress, and sorbitol to induce osmotic stress as detailed in the text. HEK293T cells stably overexpressing FLAG-EGFP control or FLAG-GGT1 were engineered using lentiviral vectors obtained through Vector Builder (Cyagen Biosciences Inc.).

mRNA Expression Analysis. Two micrograms of total RNA (RNeasy MicroKit; Qiagen Inc.) were retrotranscribed with the High-Capacity cDNA Reverse Transcription kit (Applied Biosystems). Eighty nanograms of cDNA per reaction were run using TaqMan probes (Applied Biosystems).

Statistical Analyses. Mann–Whitney test and two-way ANOVA with Bonferroni correction were used for in vitro studies (GraphPad Prism version 5.04 for Windows; GraphPad Software, www.graphpad.com). Significance was defined as $P < 0.05$.

ACKNOWLEDGMENTS. We thank the Tuttle Family and the National Institutes of Health (Grant R01CA216922) for their support of this work.

1. Srigley JR, et al.; ISUP Renal Tumor Panel (2013) The International Society of Urological Pathology (ISUP) Vancouver classification of renal neoplasia. *Am J Surg Pathol* 37:1469–1489.
2. Schmidt LS, Linehan WM (2016) Genetic predisposition to kidney cancer. *Semin Oncol* 43:566–574.
3. Keegan KA, et al. (2012) Histopathology of surgically treated renal cell carcinoma: survival differences by subtype and stage. *J Urol* 188:391–397.
4. Amin MB, et al. (2008) Chromophobe renal cell carcinoma: histomorphologic characteristics and evaluation of conventional pathologic prognostic parameters in 145 cases. *Am J Surg Pathol* 32:1822–1834.
5. Klatte T, et al. (2008) Pathobiology and prognosis of chromophobe renal cell carcinoma. *Urol Oncol* 26:604–609.
6. Kovacs A, Storkel S, Thoenes W, Kovacs G (1992) Mitochondrial and chromosomal DNA alterations in human chromophobe renal cell carcinomas. *J Pathol* 167:273–277.
7. Tickoo SK, et al. (2000) Ultrastructural observations on mitochondria and microvesicles in renal oncocytoma, chromophobe renal cell carcinoma, and eosinophilic variant of conventional (clear cell) renal cell carcinoma. *Am J Surg Pathol* 24: 1247–1256.
8. Zbar B, et al. (2002) Risk of renal and colonic neoplasms and spontaneous pneumothorax in the Birt-Hogg-Dubé syndrome. *Cancer Epidemiol Biomarkers Prev* 11: 393–400.
9. Toro JR, et al. (2008) BHD mutations, clinical and molecular genetic investigations of Birt-Hogg-Dubé syndrome: a new series of 50 families and a review of published reports. *J Med Genet* 45:321–331.
10. Menko FH, et al.; European BHD Consortium (2009) Birt-Hogg-Dubé syndrome: diagnosis and management. *Lancet Oncol* 10:1199–1206.
11. Yang P, et al. (2014) Renal cell carcinoma in tuberous sclerosis complex. *Am J Surg Pathol* 38:895–909.
12. Henske EP, Jóźwiak S, Kingswood JC, Sampson JR, Thiele EA (2016) Tuberous sclerosis complex. *Nat Rev Dis Primers* 2:16035.
13. Paner GP, et al. (2010) A novel tumor grading scheme for chromophobe renal cell carcinoma: prognostic utility and comparison with Fuhrman nuclear grade. *Am J Surg Pathol* 34:1233–1240.
14. Vera-Badillo FE, Conde E, Duran I (2012) Chromophobe renal cell carcinoma: a review of an uncommon entity. *Int J Urol* 19:894–900.
15. Young AN, et al. (2001) Expression profiling of renal epithelial neoplasms: a method for tumor classification and discovery of diagnostic molecular markers. *Am J Pathol* 158:1639–1651.
16. Weinstein JN, et al.; Cancer Genome Atlas Research Network (2013) The cancer genome atlas pan-cancer analysis project. *Nat Genet* 45:1113–1120.
17. Durinck S, et al. (2015) Spectrum of diverse genomic alterations define non-clear cell renal carcinoma subtypes. *Nat Genet* 47:13–21.
18. Davis CF, et al.; The Cancer Genome Atlas Research Network (2014) The somatic genomic landscape of chromophobe renal cell carcinoma. *Cancer Cell* 26:319–330.
19. Soga T, et al. (2006) Differential metabolomics reveals ophthalmic acid as an oxidative stress biomarker indicating hepatic glutathione consumption. *J Biol Chem* 281: 16768–16776.
20. Carretero A, et al. (2014) In vitro/in vivo screening of oxidative homeostasis and damage to DNA, protein, and lipids using UPLC/MS-MS. *Anal Bioanal Chem* 406: 5465–5476.
21. Mayr JA, et al. (2008) Loss of complex I due to mitochondrial DNA mutations in renal oncocytoma. *Clin Cancer Res* 14:2270–2275.
22. Simonnet H, et al. (2003) Mitochondrial complex I is deficient in renal oncocytomas. *Carcinogenesis* 24:1461–1466.
23. Hakimi AA, et al. (2016) An integrated metabolic atlas of clear cell renal cell carcinoma. *Cancer Cell* 29:104–116.
24. Anonymous; Cancer Genome Atlas Research Network (2013) Comprehensive molecular characterization of clear cell renal cell carcinoma. *Nature* 499:43–49.
25. Gerharz CD, et al. (1995) Establishment and characterization of two divergent cell lines derived from a human chromophobe renal cell carcinoma. *Am J Pathol* 146: 953–962.
26. Barretina J, et al. (2012) The Cancer Cell Line Encyclopedia enables predictive modelling of anticancer drug sensitivity. *Nature* 483:603–607.
27. Rhodes DR, et al. (2007) Oncomine 3.0: genes, pathways, and networks in a collection of 18,000 cancer gene expression profiles. *Neoplasia* 9:166–180.
28. Will Y, et al. (2000) gamma-glutamyltranspeptidase-deficient knockout mice as a model to study the relationship between glutathione status, mitochondrial function, and cellular function. *Hepatology* 32:740–749.
29. Joshi S, et al. (2015) The genomic landscape of renal oncocytoma identifies a metabolic barrier to tumorigenesis. *Cell Reports* 13:1895–1908.
30. Fischer P, Störkel S, Haase W, Scherberich JE (1991) Differential diagnosis of histogenetically distinct human epithelial renal tumours with a monoclonal antibody against gamma-glutamyltransferase. *Cancer Immunol Immunother* 33:382–388.
31. Chapman MA, et al. (2011) Initial genome sequencing and analysis of multiple myeloma. *Nature* 471:467–472.
32. Cibulskis K, et al. (2013) Sensitive detection of somatic point mutations in impure and heterogeneous cancer samples. *Nat Biotechnol* 31:213–219.
33. Priolo C, et al. (2014) AKT1 and MYC induce distinctive metabolic fingerprints in human prostate cancer. *Cancer Res* 74:7198–7204.
34. Parkhitko AA, et al. (2014) Autophagy-dependent metabolic reprogramming sensitizes TSC2-deficient cells to the antimetabolite 6-aminonicotinamide. *Mol Cancer Res* 12:48–57.
35. Priolo C, et al. (2015) Tuberous sclerosis complex 2 loss increases lysophosphatidylcholine synthesis in lymphangioleiomyomatosis. *Am J Respir Cell Mol Biol* 53: 33–41.